Supporting Information

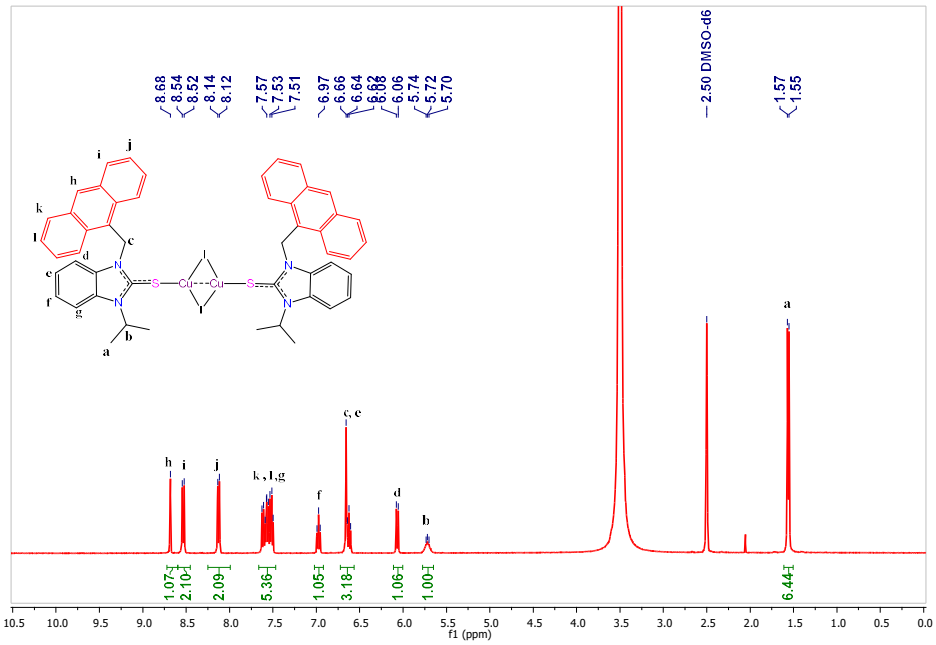

Fig. S1. ^{1}H NMR spectrum of **1** in DMSO-d_6 at 25 °C.

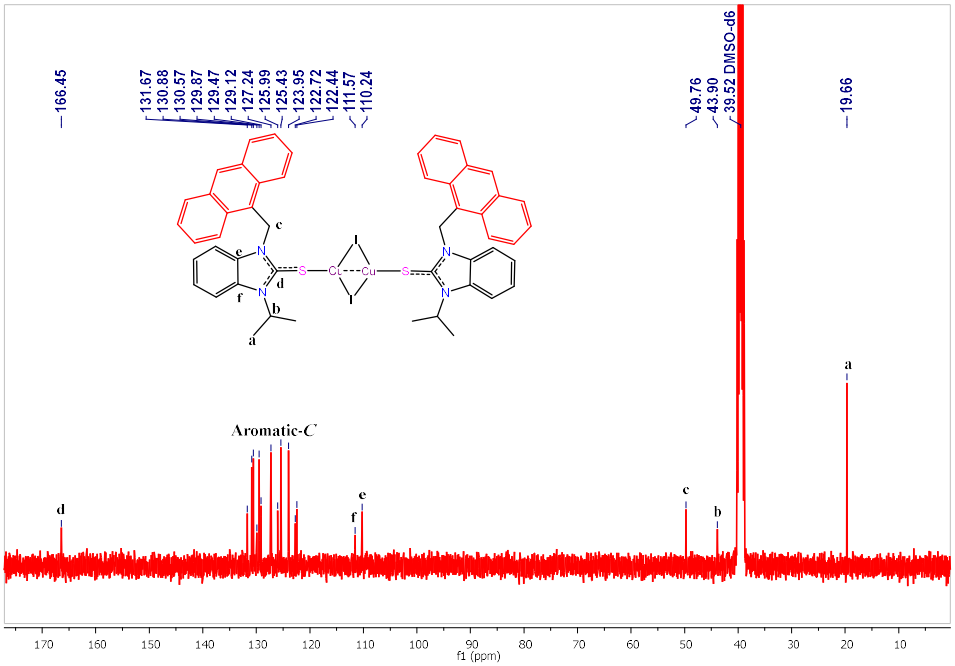

Fig. S2. ^{13}C NMR spectrum of **1** in DMSO-d_6 at 25 °C.

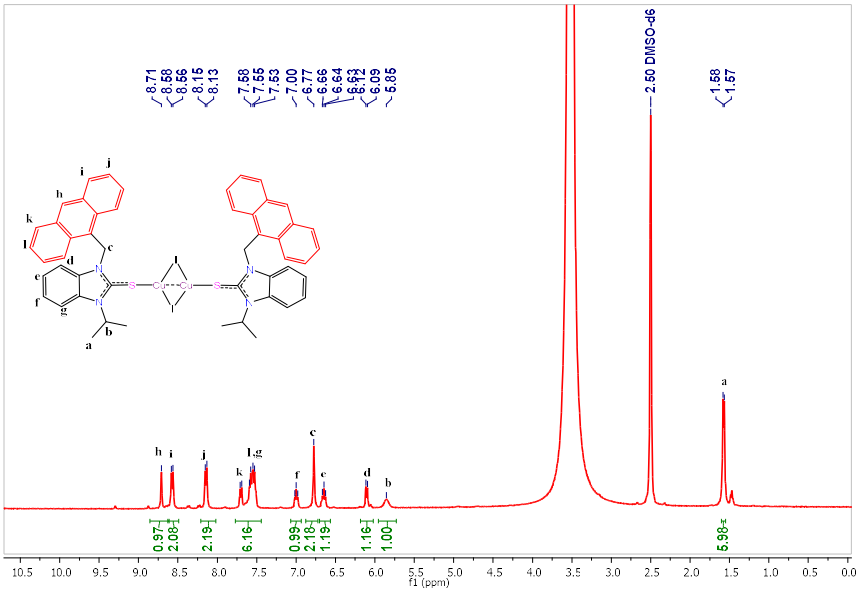

Fig. S3. ^{1}H NMR spectrum of **2** in DMSO-d_6 at 25 °C.

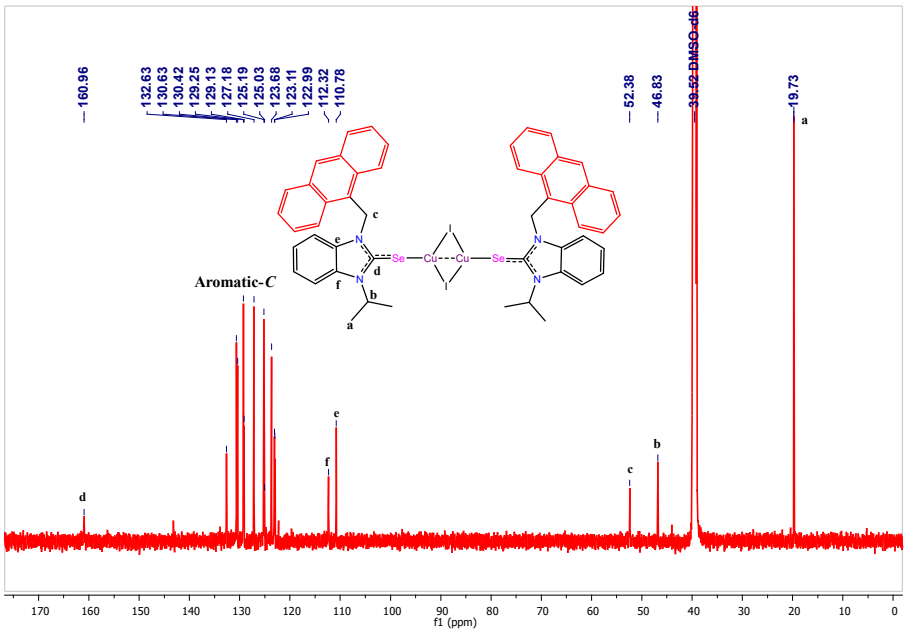

Fig. S4. ^{13}C NMR spectrum of **2** in DMSO-d_6 at 25 °C.

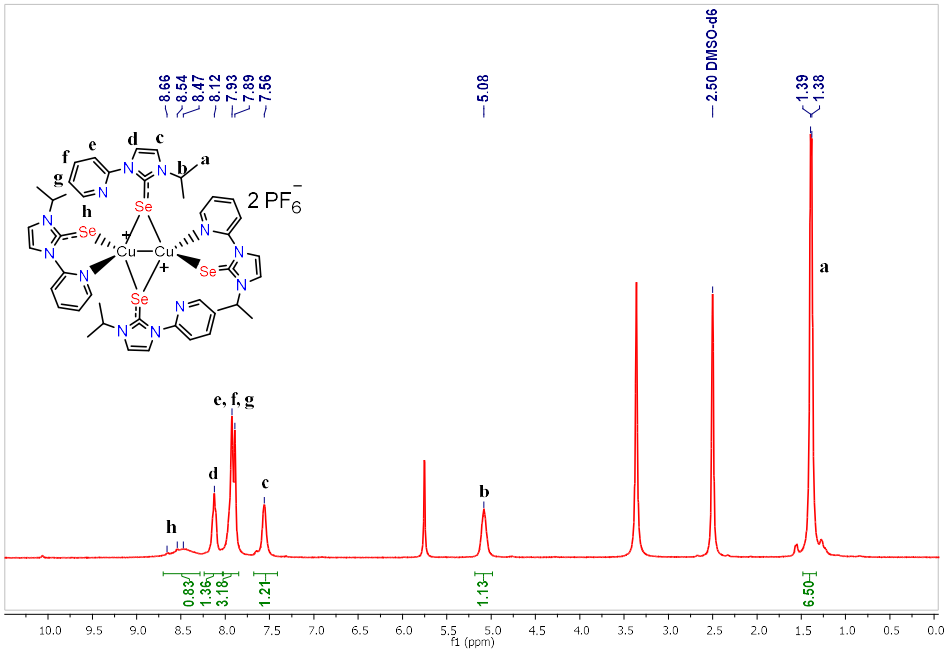

Fig. S5. ^{1}H NMR spectrum of **3** in DMSO-d_6 at 25 °C.

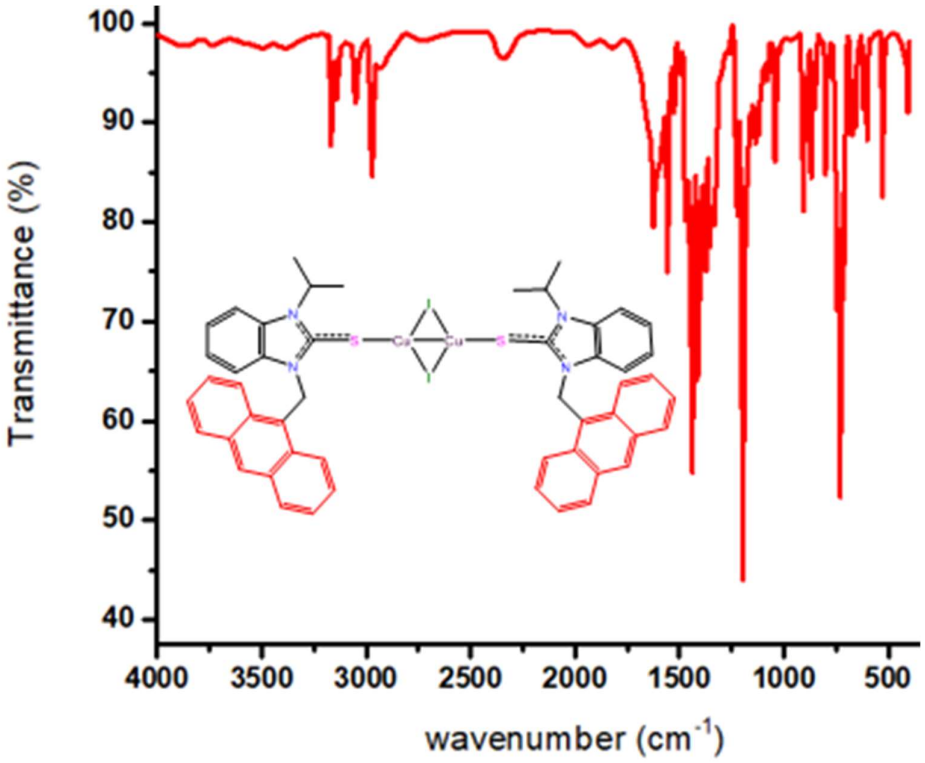

Fig. S6. FT-IR spectrum of **1** at 25 °C (KBr method).

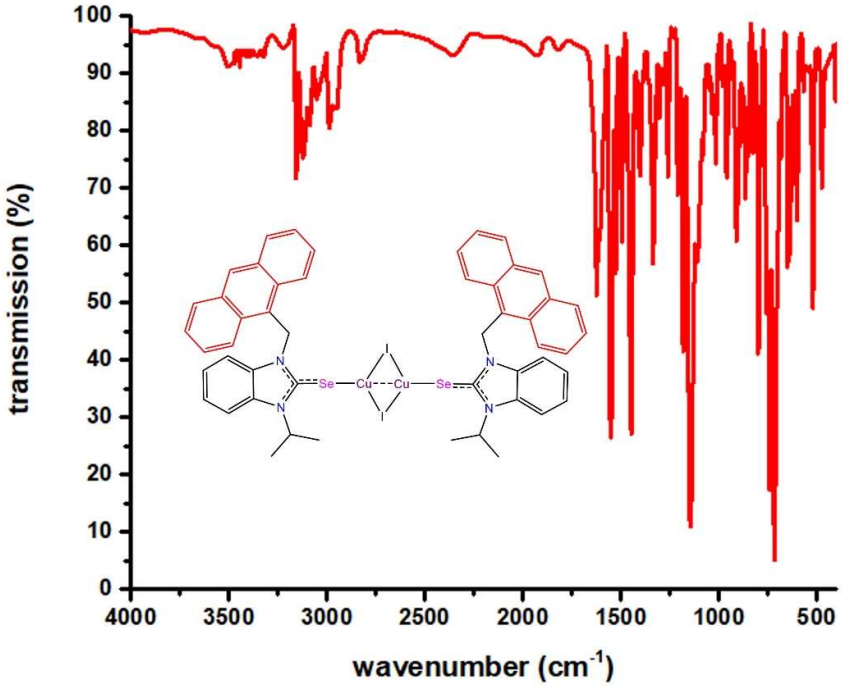

Fig. S7. FT-IR spectrum of **2** at 25 °C (neat).

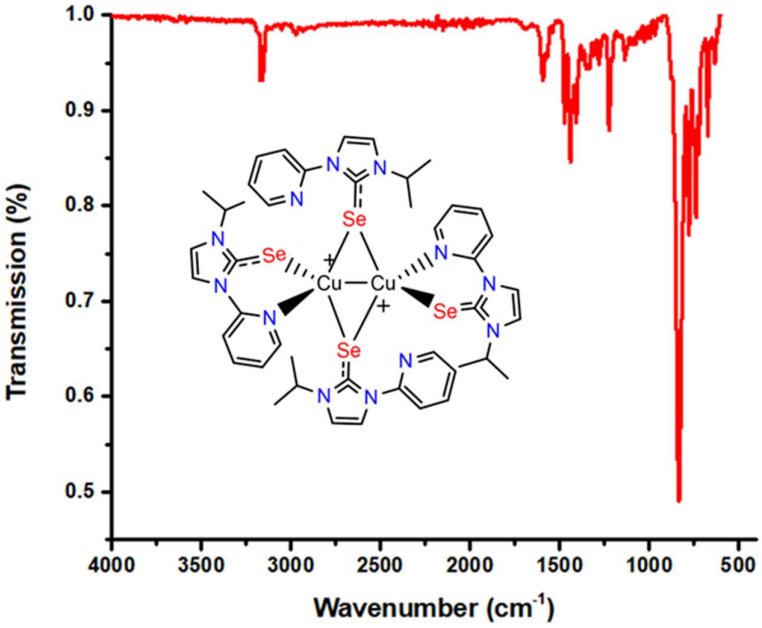

Fig. S8. FT-IR spectrum of **3** at 25 °C (neat).

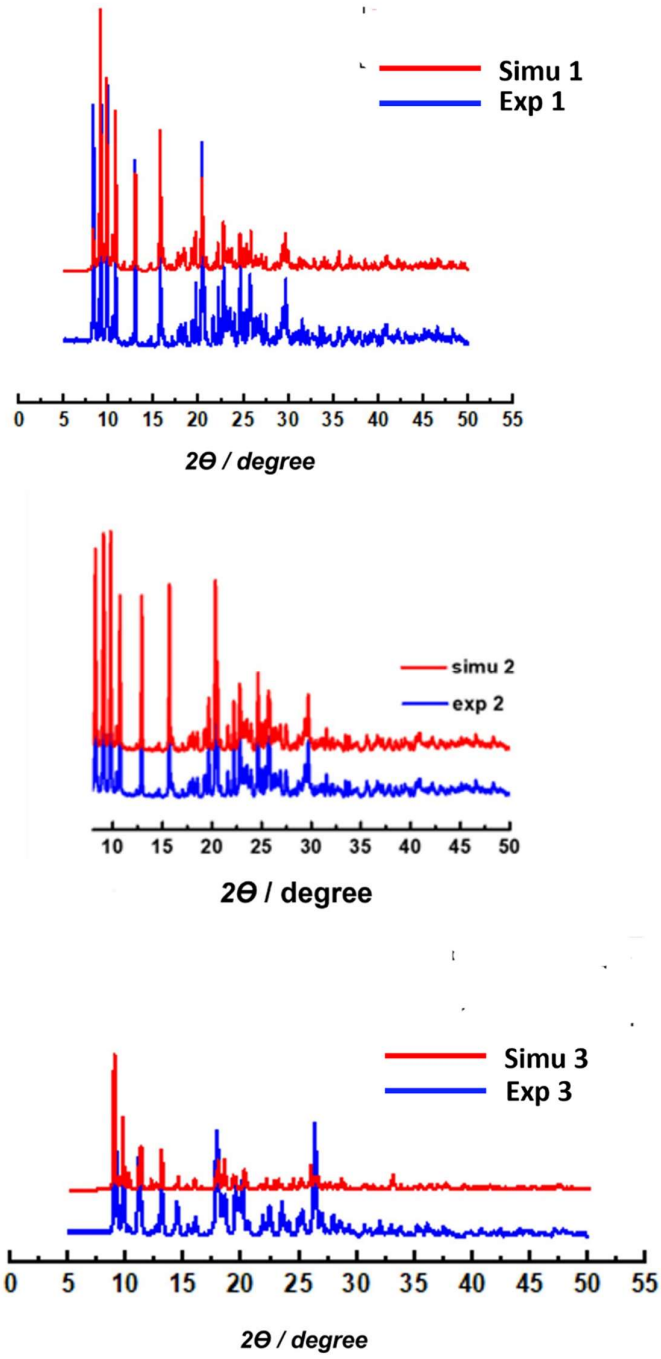

Fig. S9. Powder XRD data analysis of **1-3**.

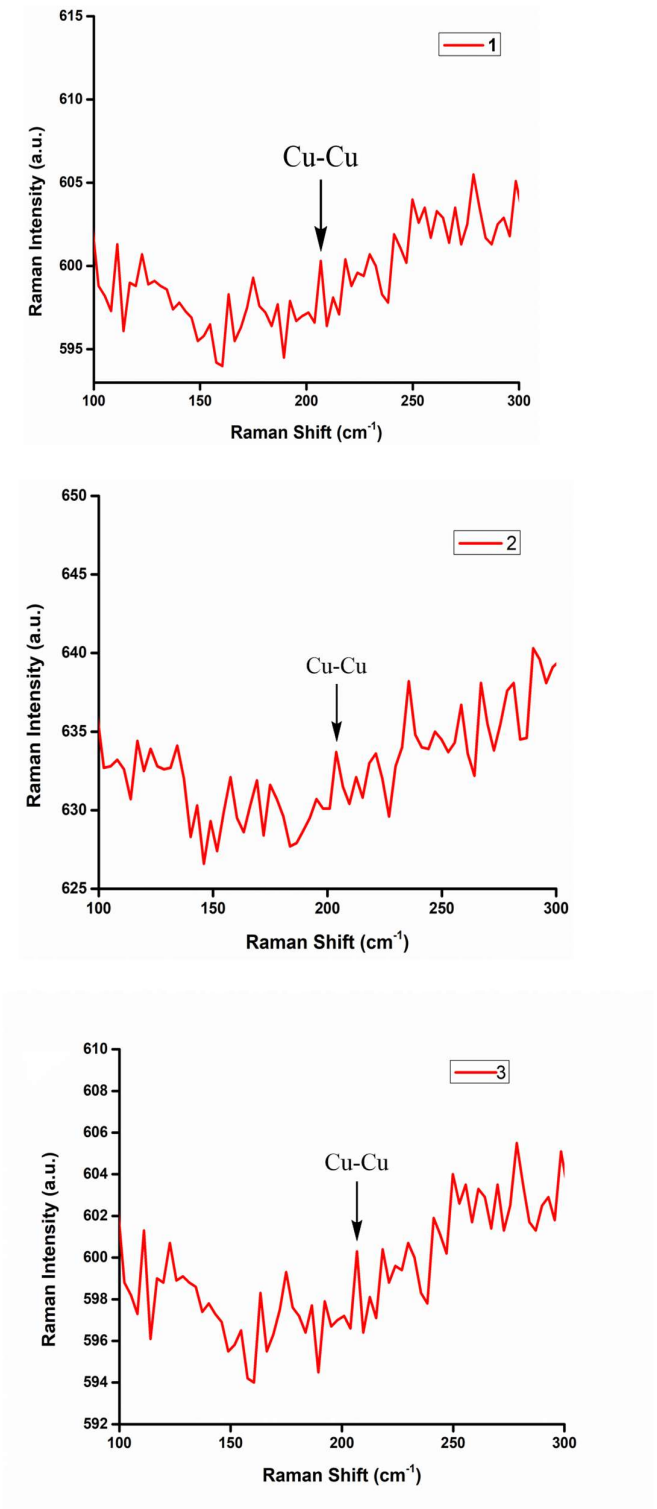

Fig. S10. Raman spectra of **1-3**.

We have characterised **1-3** using the Raman spectroscopy and reported the spectra in the range 100-300 cm^{-1}. We observed the weak signals for our samples. Unfortunately, the samples are unstable under high laser power to get better signals to noise ratio. Moreover, the copper(I)-

copper(I) interaction is known to give very weak signal at 206 cm^{-1} (Ref. N. V. S. Harisomayajula, B.H. Wu, D.Y. Lu, T.-S. Kuo, I.C. Chen, Y.C. Tsai, *Angew. Chem. Int. Ed*. 2018, **57**, 9925-9932). By considering the sample stability under the laser power, we have collected the Raman data. We got the Cu-Cu bond at 206 cm^{-1}, which is comparable with literature Cu-Cu bond at 204 cm^{-1}.

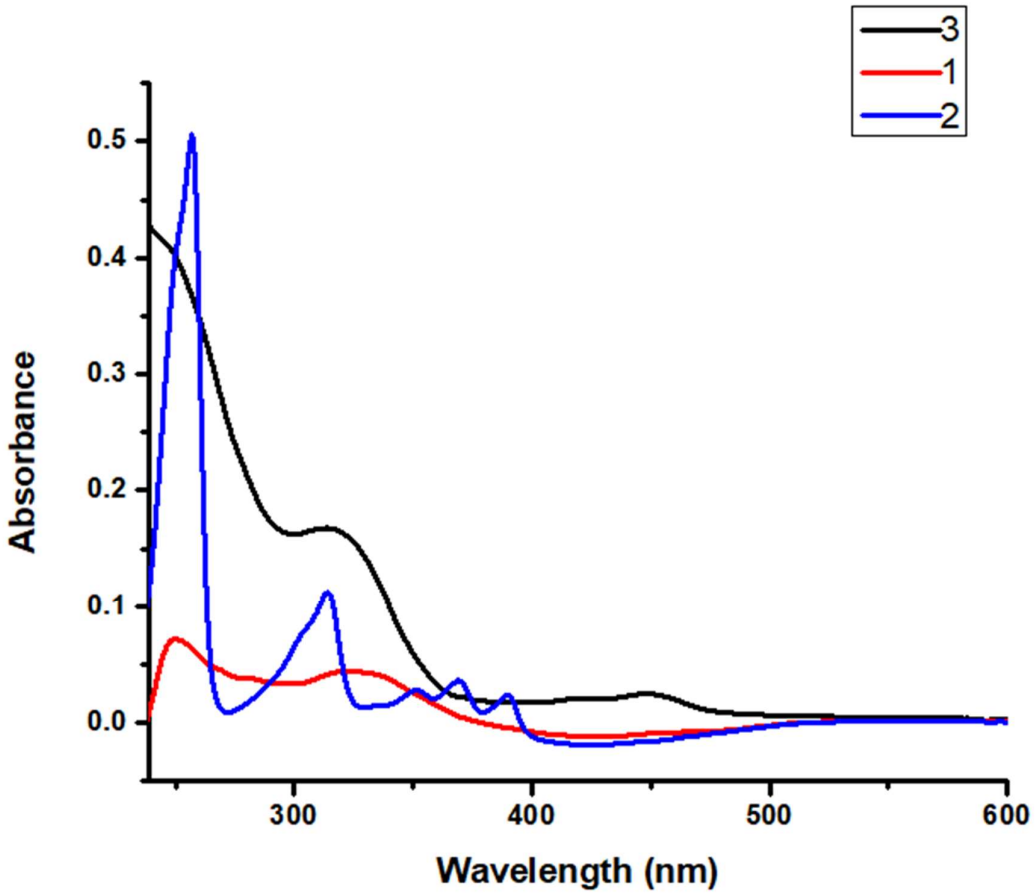

Fig. S11. UV-vis spectra of **1**-**3**. (1×10^{-6} M THF).

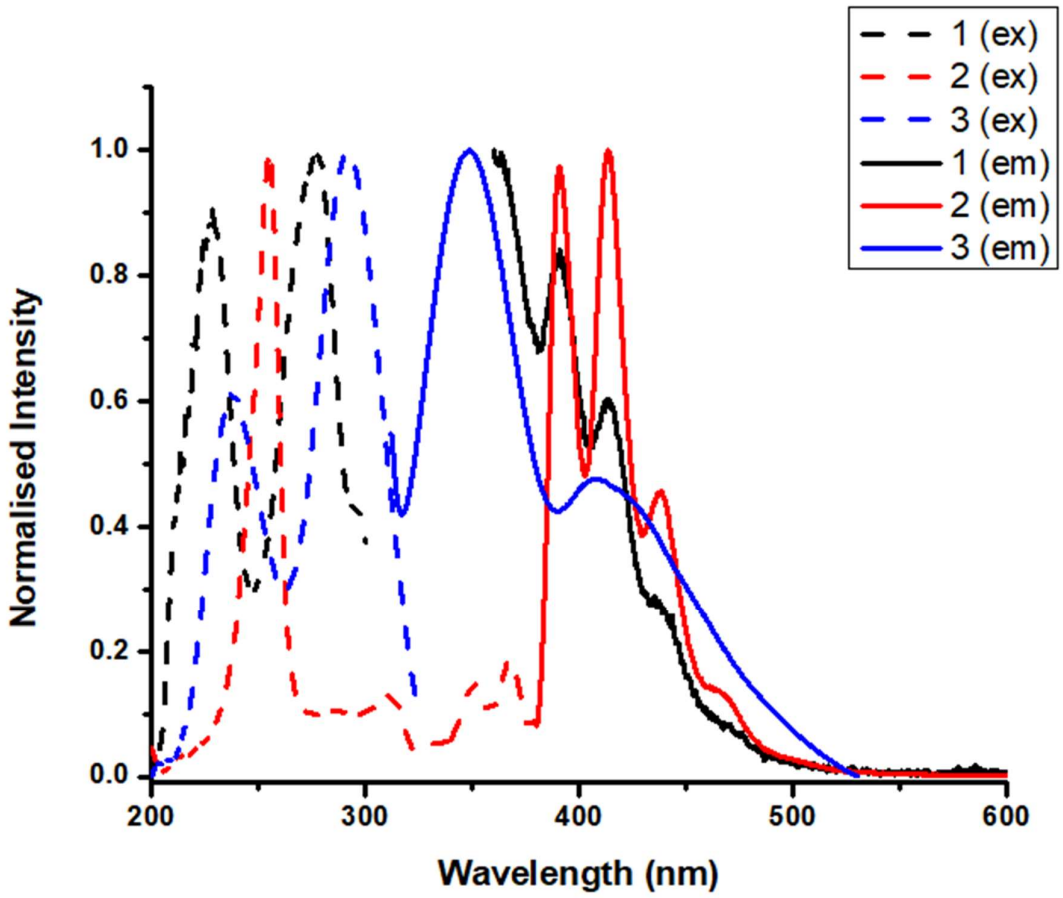

Fig. S12. Emission spectra of **1-3 in** solution state. Dash line-Ex spectra. Solid line-Em spectra (1×10^{-6} M THF). See Table S4.

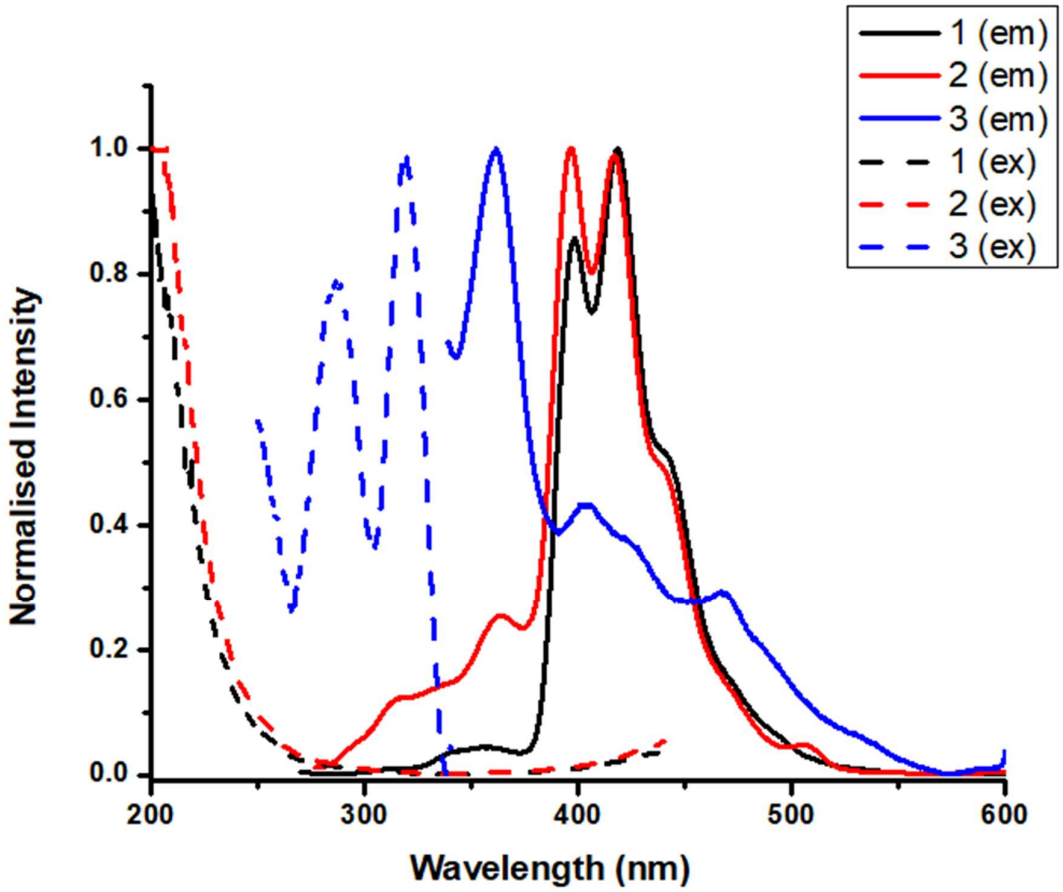

Fig. S13. Emission spectra of **1-3** in solid state. Dash line-Ex spectra. Solid line-Em spectra (Crystalline state). See Table S4.

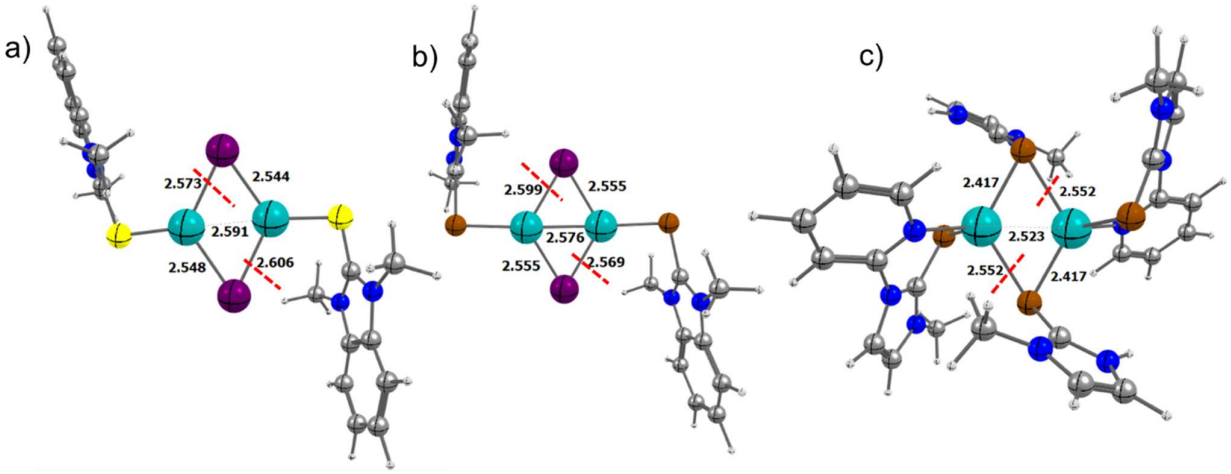

Fig. S14. Hydrogen-optimised truncated models of complex highlighting the two LCuI/LCuSe fragments of complexes **1** (a), **2** (b), **3** (c).

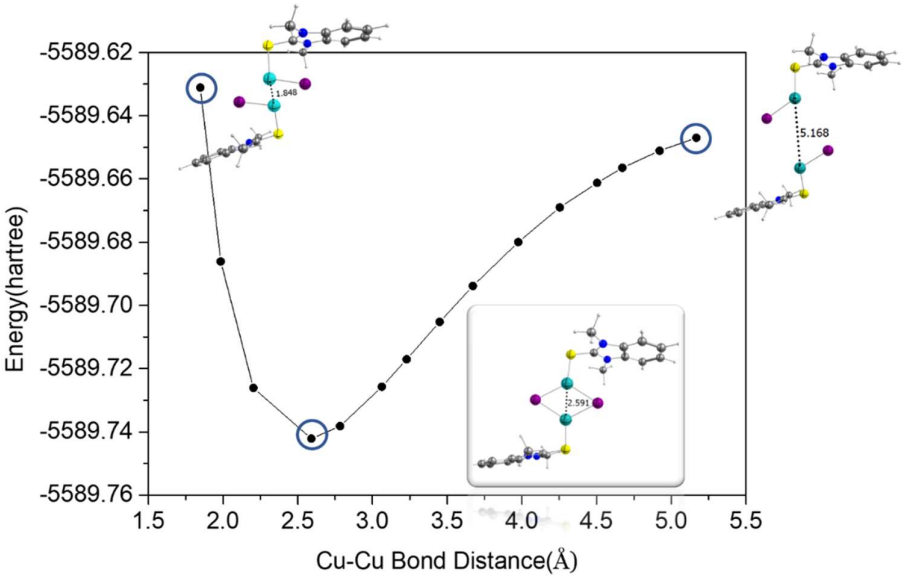

Fig. S15. DFT computed potential energy scan (PES) surface by scanning Cu…Cu bond distance in **1**.Colour code: grey (carbon); red (oxygen); blue (nitrogen); violet (iodine); hydrogen (white); cyan (copper); yellow (sulphur).

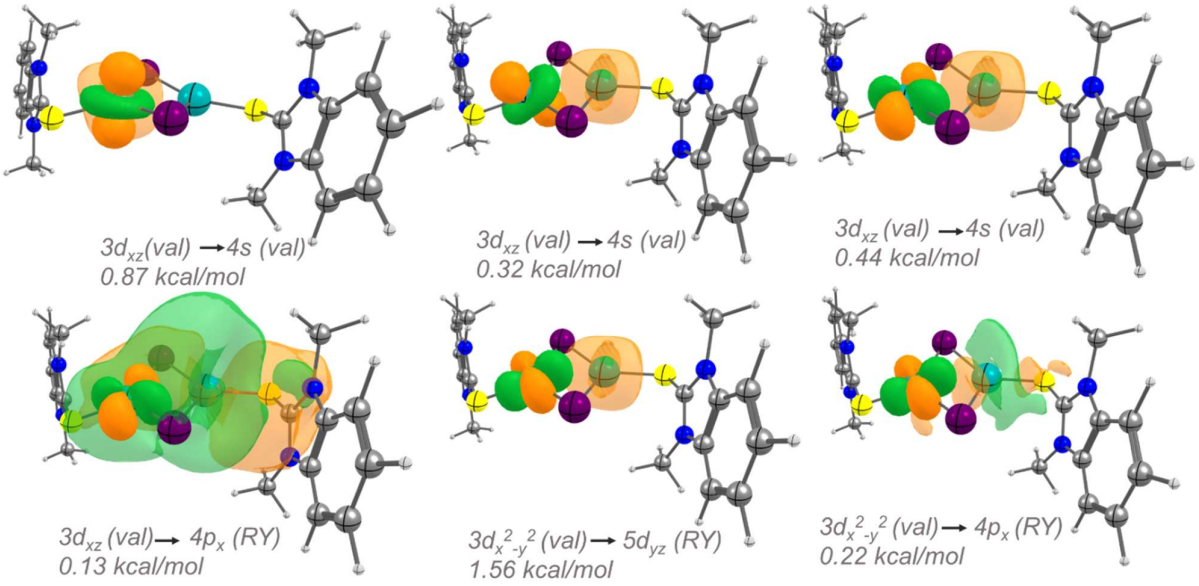

Fig. S16. NBO computed Second-order perturbation donor-acceptor interaction representing the strength of the Cu-Cu (d^{10}-d^{10}) interaction in complex **1**. Colour code: grey (carbon); red (oxygen); blue (nitrogen); violet (iodine); hydrogen (white); cyan (copper); yellow (sulphur).

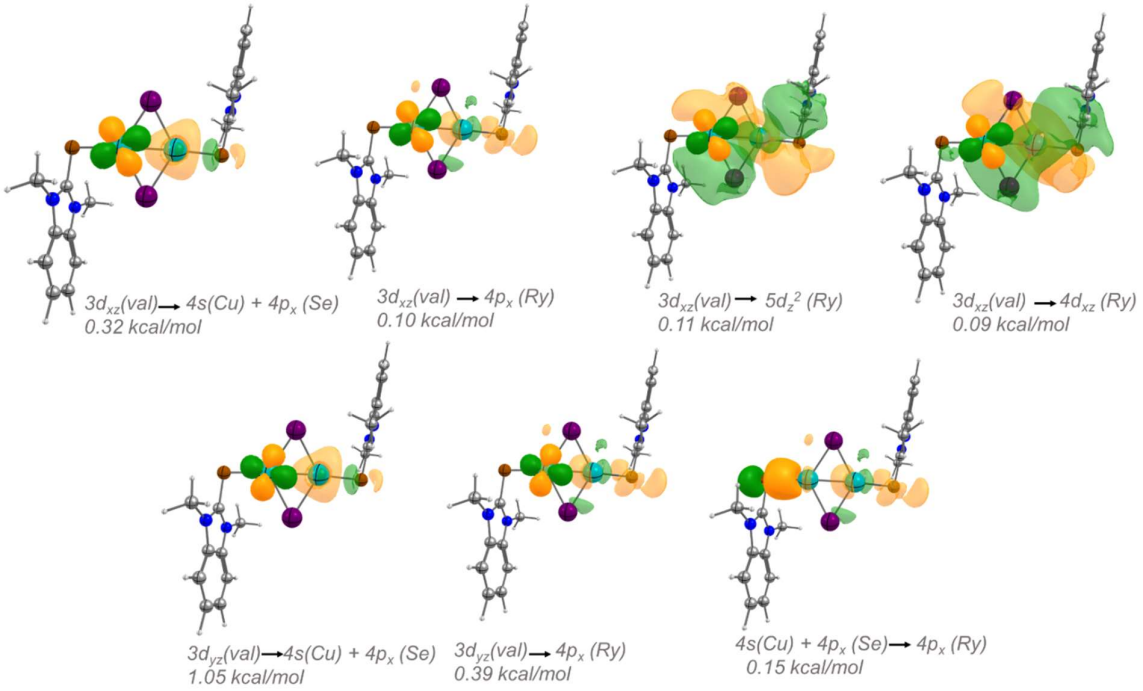

Fig. S17. NBO computed Second order perturbation donor acceptor interaction representing the strength of the Cu-Cu (d^{10}-d^{10}) interaction in complex **2**. Colour code: grey (carbon); red (oxygen); blue (nitrogen);violet (iodine);hydrogen (white);cyan (copper);brown (selenium).

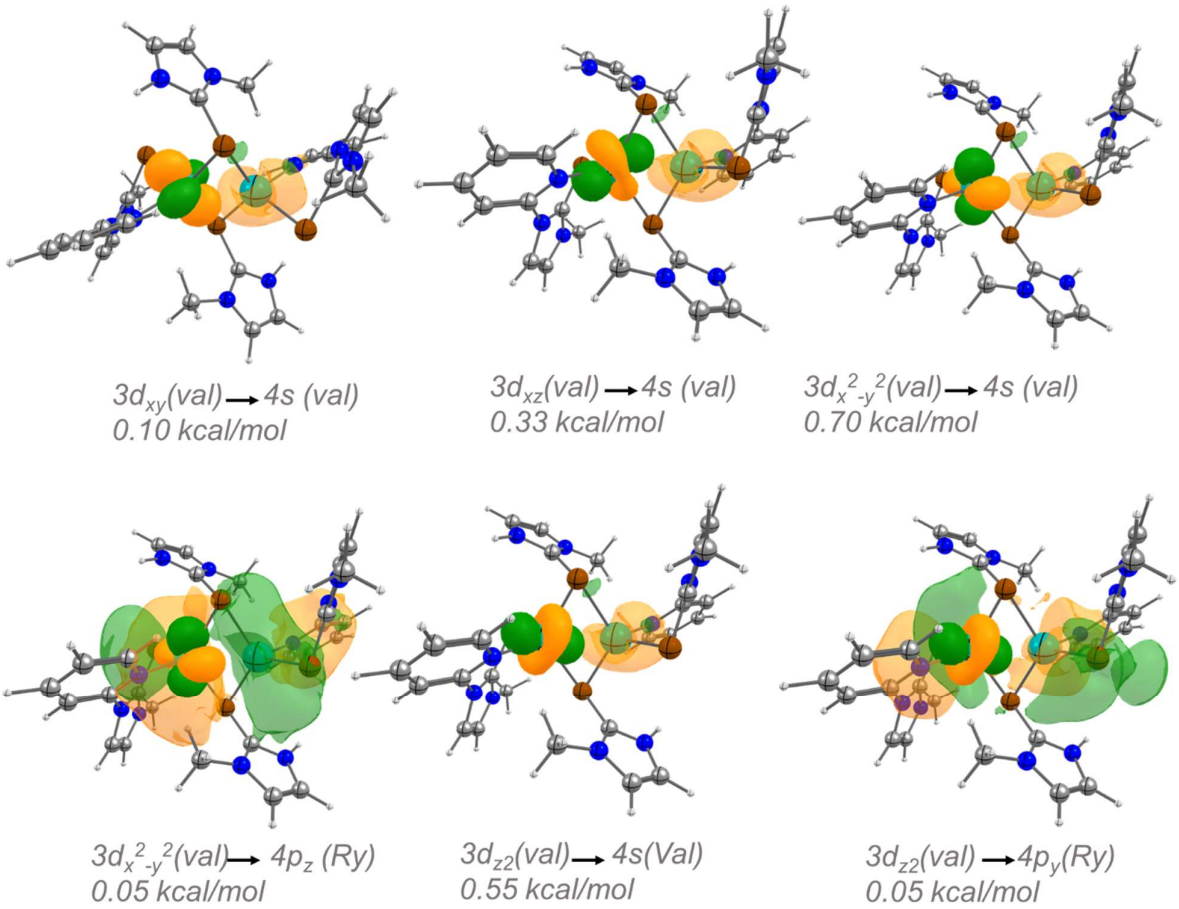

Fig. S18. NBO computed Second order perturbation donor acceptor interaction representing the strength of the Cu-Cu(d^{10}-d^{10}) interaction in complex **3**. Colour code: grey(carbon); red(oxygen);blue(nitrogen);violet(iodine);hydrogen(white);cyan(copper);brown(selenium).

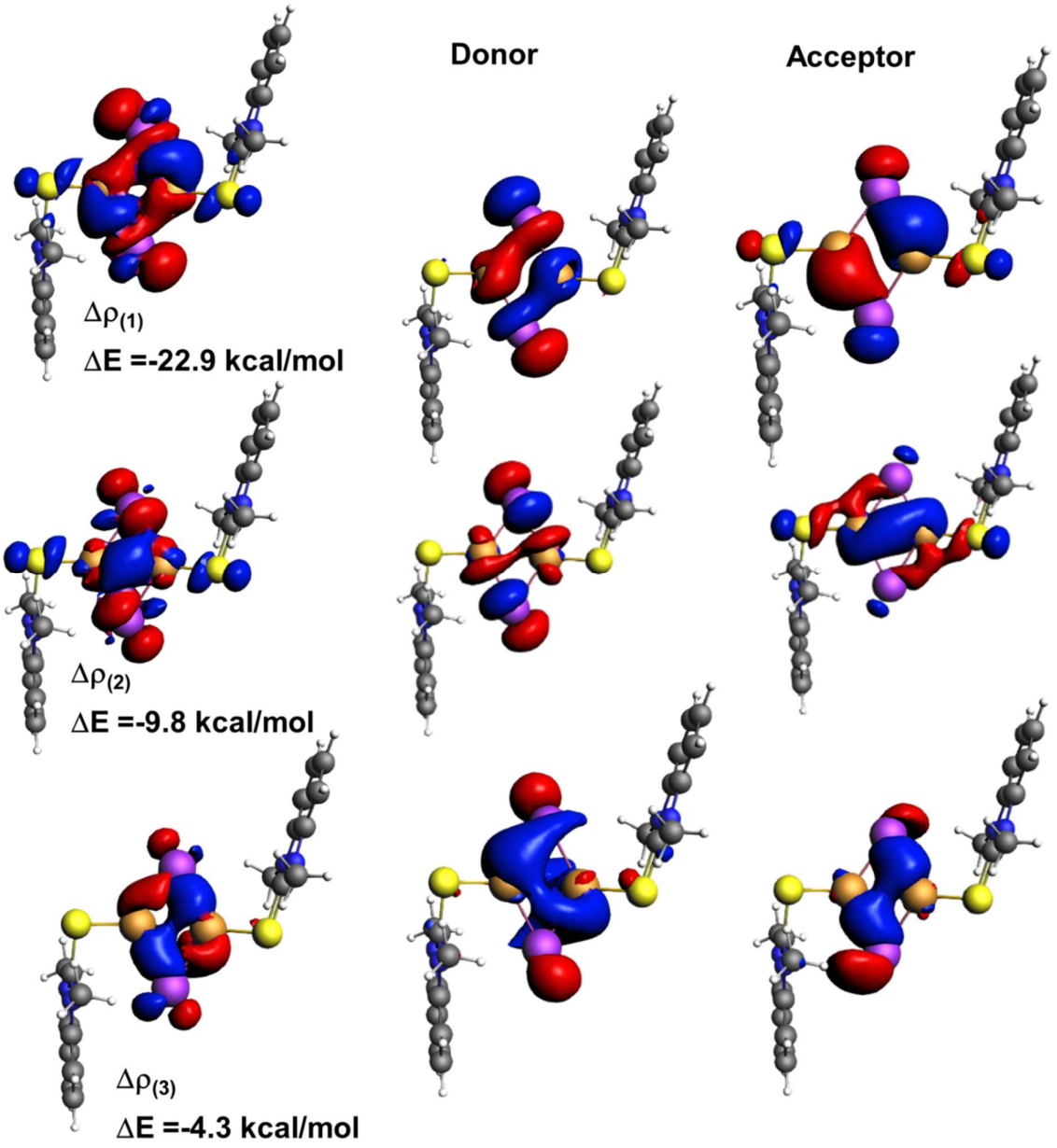

Fig. S19. Plots of deformation densities $\Delta\rho_n$ and the orbital stabilization energies ΔE of complex **1**. The isosurface value for deformation densities is 0.0003. The direction of the deformation density plot is from red to blue.

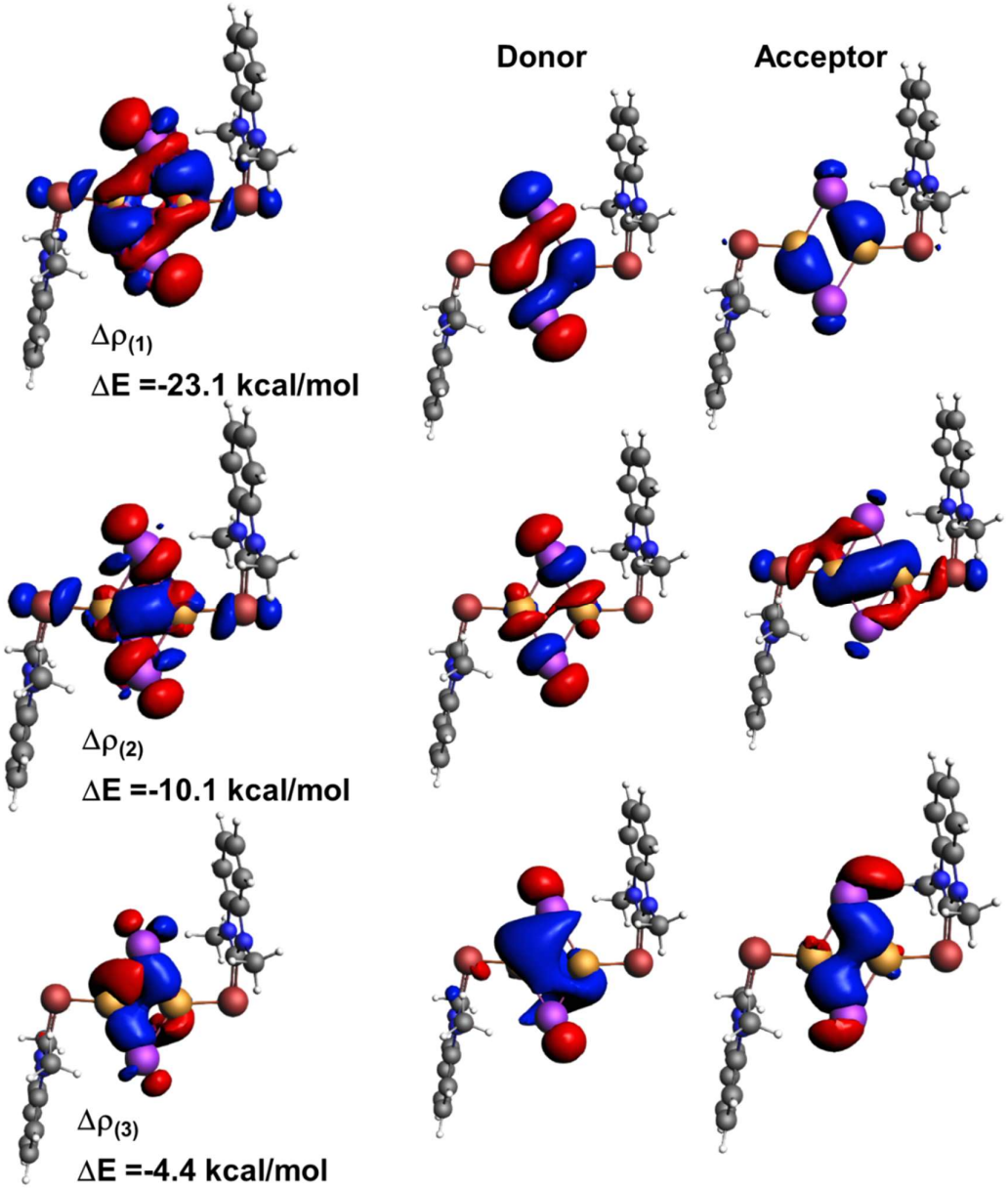

Figure S20: Plots of deformation densities $\Delta\rho_n$ and the orbital stabilization energies ΔE of complex **2**. The isosurface value for deformation densities is 0.0003. The direction of the deformation density plot is from red to blue.

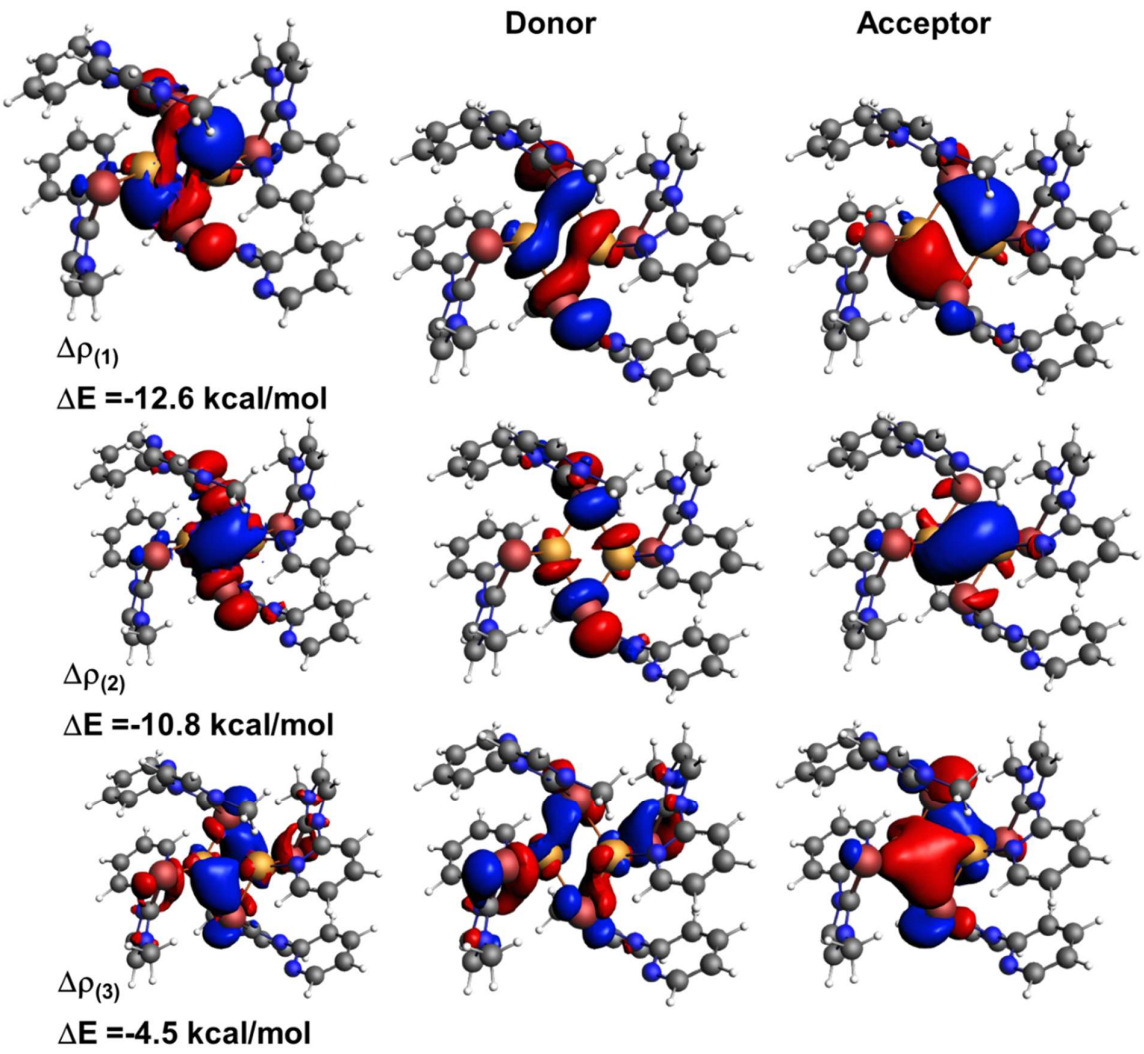

Figure S21: Plots of deformation densities $\Delta\rho_n$ and the orbital stabilization energies ΔE of complex **3**. The isosurface value for deformation densities is 0. 0003. The direction of the deformation density plot is from red to blue.

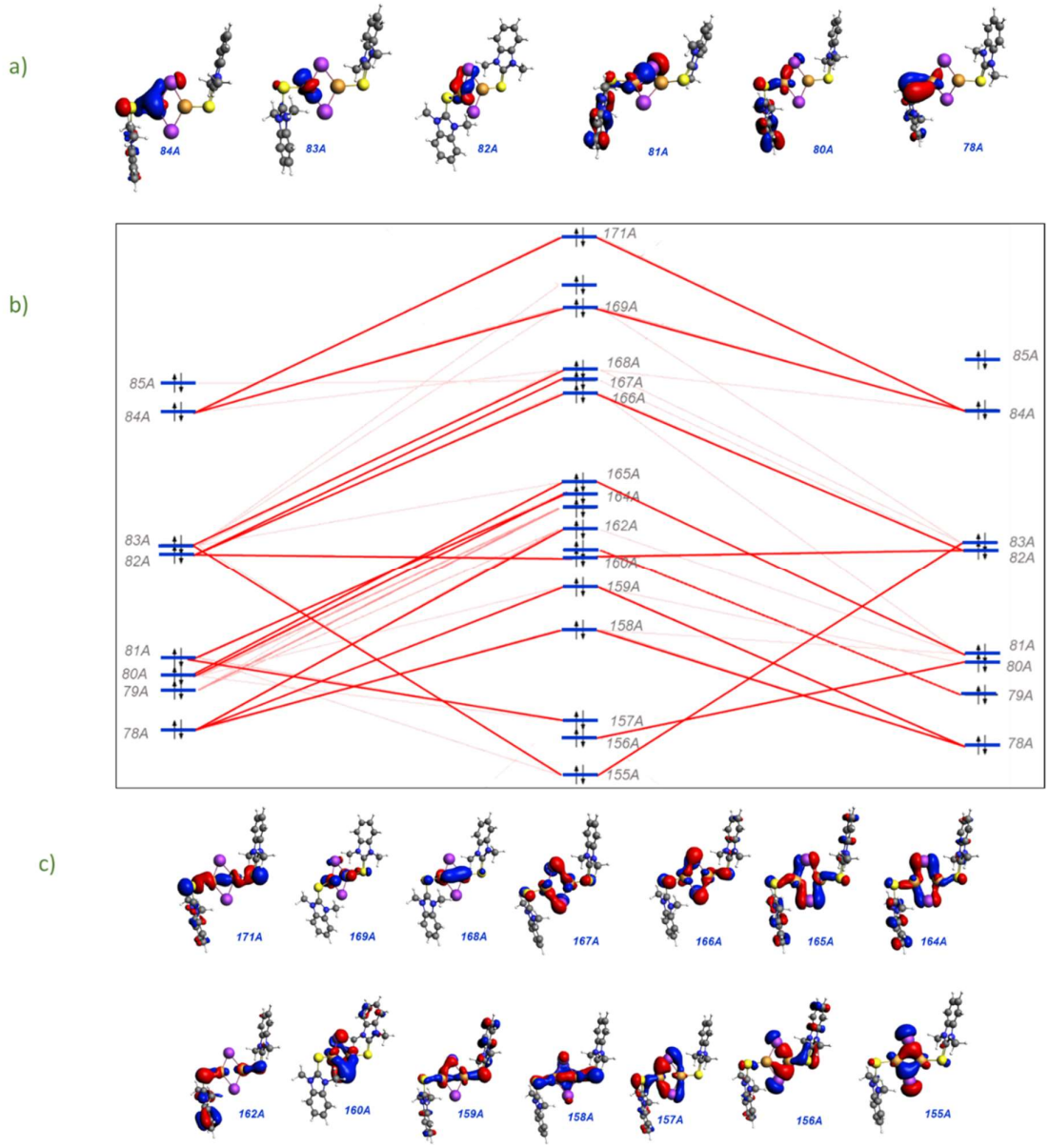

Figure S22: (a) Atomic orbitals corresponding to the Cu orbitals in complex **1**. (b) Molecular energy level diagram for complex **1**. (c) Molecular orbitals corresponding to the Cu-Cu interactions of Cu AO's.

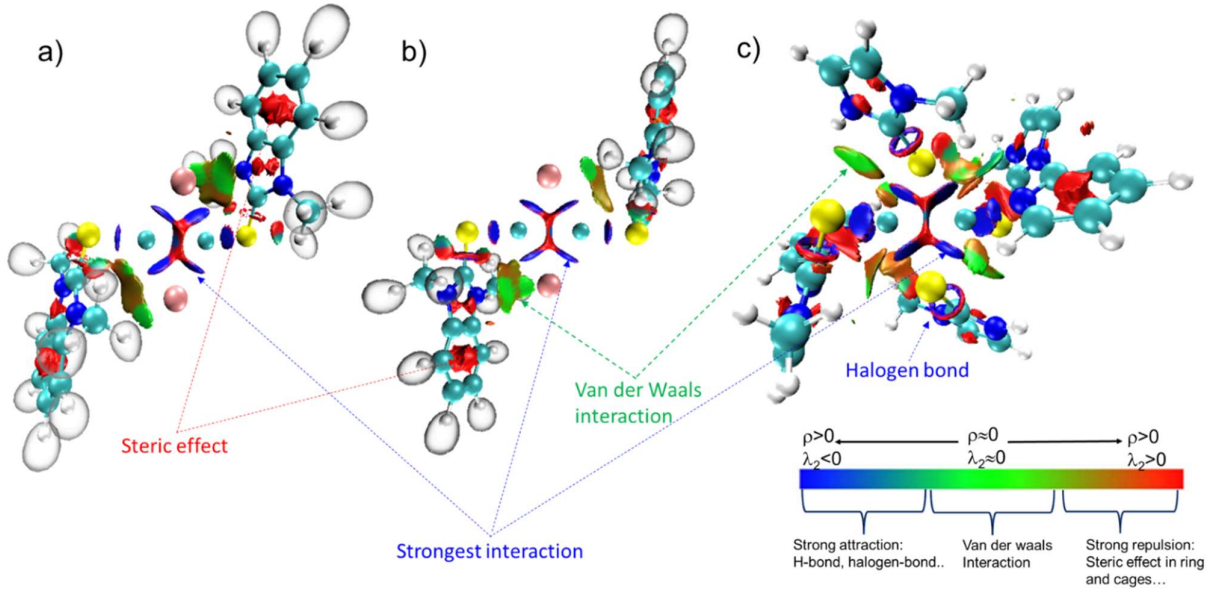

Figure S23: Reduced density gradient (RDG) analysis for complexes **1** (a), **2** (b), **3** (c).

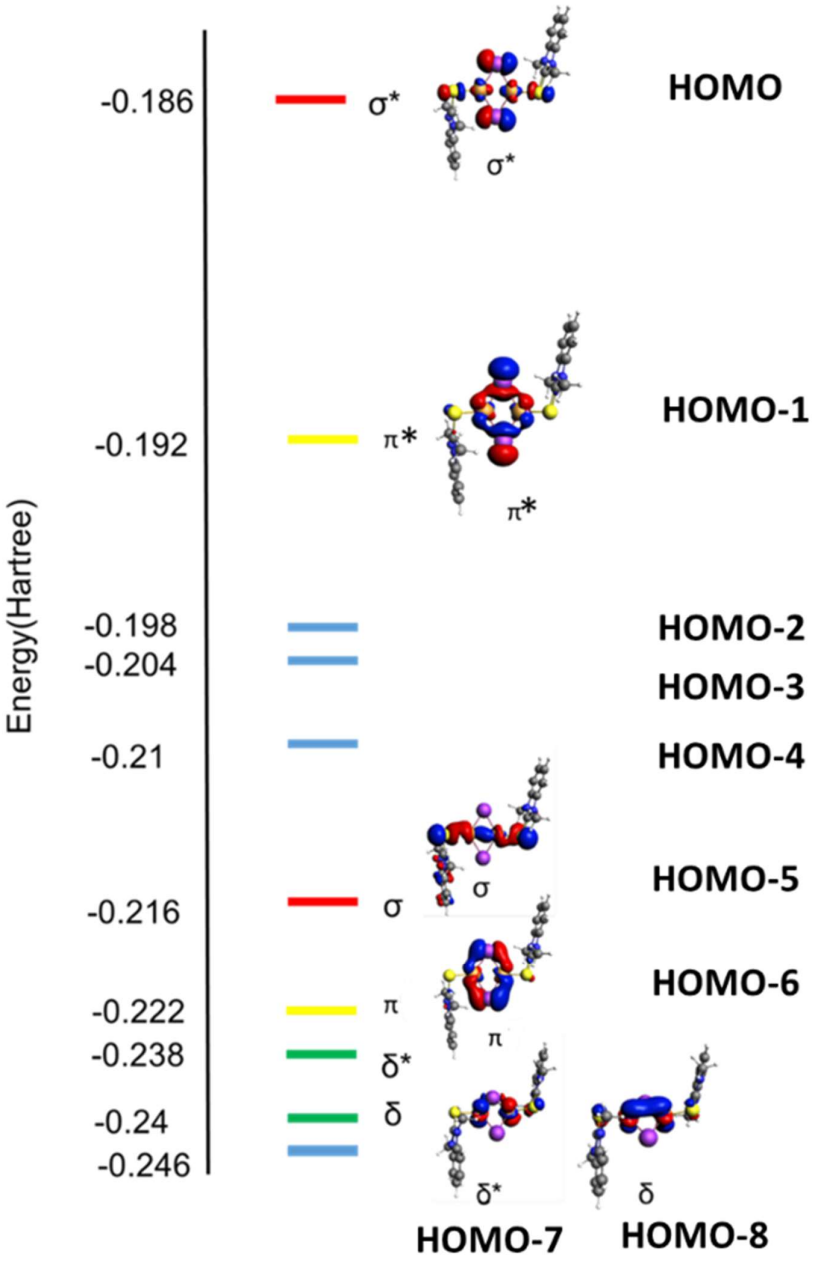

Figure S24. Frontier molecular orbitals of complex **1**, representing different σ π δ interactions.

Table S1. The structural parameters of compounds **1-3**.

	1	**2**	**3**
Empirical Formula	$C_{50}H_{44}Cu_2I_2N_4S_2$	$C_{50}H_{44}Cu_2I_2N_4Se_2$	$C_{46}H_{54}Cl_6Cu_{1.98}F_{12}N_{12}P_2Se_{3.99}$
Formula Weight	1145.89	1239.69	1718.51
Temperature/K	298.0	298.0	298
Crystal System	triclinic	triclinic	monoclinic
Space Group	P-1	P-1	$P2_1/n$
a/Å	10.4449(3)	10.4551(17)	11.441(6)
b/Å	11.2293(3)	11.2312(17)	10.490(6)
c/Å	21.4005(6)	21.572(3)	27.824(15)
α/°	93.5040(10)	93.703(5)	90
β/°	94.2160(10)	93.917(5)	101.830(17)
γ/°	111.4220(10)	111.497(5)	90
Volume/A^3	2319.83(11)	2340.3(6)	3268(3)
Z	2	2	2
ρ_{calc}/g^3	1.640	1.759	1.746
μ/mm^{-1}	2.376	3.822	3.238
F(000)	1136.0	1208.0	1694.0
Crystal size/mm^3	0.2 × 0.03 × 0.02	0.35 × 0.3 × 0.27	0.09 × 0.09 × 0.09
Radiation	MoKα (λ = 0.71073)	MoKα (λ = 0.71073)	MoKα (λ = 0.71073)
2Θ range for data collection/°	3.834 to 54.268	3.916 to 54.27	4.162 to 54.366
Index ranges	$-13 \leq h \leq 13$, $-14 \leq k \leq 14$, $-27 \leq l \leq 27$	$-13 \leq h \leq 13$, $-14 \leq k \leq 14$, $-27 \leq l \leq 27$	$-14 \leq h \leq 14$, $-13 \leq k \leq 13$, $-34 \leq l \leq 35$
Reflections collected	47194	53681	28414
Independent reflections	10254 [R_{int} = 0.0343, R_{sigma} = 0.0284]	10311 [R_{int} = 0.0416, R_{sigma} = 0.0299]	7229 [R_{int} = 0.0689, R_{sigma} = 0.0695]
Data/restraints/parameters	10254/0/546	10311/0/546	7229/0/384
Goodness-of-fit on F^2	1.020	1.037	1.032
Final R indexes [I>=2σ (I)]	R_1 = 0.0291, wR_2 = 0.0623	R_1 = 0.0298, wR_2 = 0.0675	R_1 = 0.0588, wR_2 = 0.1510
Final R indexes [all data]	R_1 = 0.0453, wR_2 = 0.0677	R_1 = 0.0360, wR_2 = 0.0707	R_1 = 0.1032, wR_2 = 0.1733
Largest diff. peak/hole / e $Å^{-3}$	0.61/-0.63	0.91/-0.83	0.91/-0.82

Table S2. Selected bond lengths of **1-3** (Å)

	1	**2**	**3**	
Cu1-E1	2.2205(8)	2.3437(6)	$Se^{(1)}$ - $Cu^{(1)}$	2.4294(14)
Cu1-I1	2.5475(4)	2.5986(6)	$Cu^{(1)}$ - $Cu^{(1)1}$	2.5231(18)
Cu1-Cu2	2.5911(5)	2.5767(7)	$Se^{(1)}$ - $C^{(6)}$	1.862(5)
Cu1-E2	2.2367(8)		$Cu^{(1)}$ - $N^{(1)}$	2.082(5)
Cu2-I2	2.5439(4)	2.5689(5)	$Cu^{(1)}$ - $Se^{(2)}$	2.5522(14)
			$Cu^{(1)}$ - $Se^{(2)1}$	2.4175(14)
			$Se^{(1)}$ - $Cu^{(1)}$	2.4294(14)

Table S3. Selected bond angles of **1-3** [˚]

	1	**2**	**3**	
E1-Cu1-I1	118.88(2)	117.99(2)	$C^{(6)}$- $Se^{(1)}$ - $Cu^{(1)}$	86.62(17)
E2-Cu2-I1	117.88(2)	117.97(2)	$Se^{(1)}$ - $Cu^{(1)}$- $Cu^{(1)1}$	123.18(5)
C1-E1-Cu1	102.92(9)	92.26(9)	$Se^{(1)}$ - $Cu^{(1)}$ - $Se^{(2)}$	96.88(4)
N1-C1-E1	125.49(18)	126.7(2)	$Cu^{(1)1}$ - $Cu^{(1)}$ - $Se^{(2)}$	56.89(4)
E1-Cu1-Cu2	167.02(3)	170.71(2)	$N^{(1)}$ - $Cu^{(1)}$ - $Se^{(1)}$	94.71(13)
Cu1-I1-Cu2	58.705(12)	59.995(16)	$N^{(1)}$ - $Cu^{(1)}$ - $Cu^{(1)1}$	141.00(14)
			$N^{(1)}$ - $Cu^{(1)}$ - $Se^{(2)1}$	111.74(14)
			$N^{(1)}$ - $Cu^{(1)}$ - $Se^{(2)}$	114.67(14)
			$Se^{(2)1}$ - $Cu^{(1)}$ - $Se^{(1)}$	116.40(4)
			$Se^{(2)1}$ - $Cu^{(1)}$ - $Cu^{(1)1}$	62.16(3)
			$Se^{(2)1}$ - $Cu^{(1)}$ - $Se^{(2)}$	119.05(5)

Table S4. Photophysical properties of **1-3**.

Compound	λ_{abs}, nm	λ_{ex}, nm (solution)	λ_{em}, nm (solution)	λ_{ex}, nm (solid)	λ_{em}, nm (solid)
1	249 and 327	276	391, 417	200	400, 419
2	253, 314, 352, 369 and 389	254	414, 419, 437	204	398, 417
3	319	291	346, 407	319	360, 403

Table S5. Continuous Shape Measurement (CShM) for Cu(I) sites in Cu(I)-NHCh complexes **1** and **2**

Complex	**1**	**2**
Metal Site (ML_3)	Cu(I)	Cu(I)
TP-3	**0.235**	**0.107**
vT-3	3.239	2.936
fvOC-3	11.275	10.836
mvOC-3	8.853	9.135

TP-3: Trigonal (D3h)
vT-3: Vacant tetrahedron(C3v)
fvOC-3: fac-Trivacant octahedron (C3v)
mvOC-3: mer-Trivacant octahedron (C2v)

Table S6. Continuous Shape Measurement (CShM) for Cu(I) sites in Cu(I)-NHCh complex **3**

Complex	**3**
Metal Site (ML_4)	Cu(I)
SP-4	28.146
T-4	**1.682**
SS-4	8.126
vTBPY-4	2.983

SP-4: Square (D4h)
T-4: Tetrahedron(Td)
SS-4: Seesaw(C2v)
vTBPY-4: Vacant trigonal bipyramid(C3v)